

## Article

# Thermoplastic Materials for the Metal Replacement of Non-Structural Components in Marine Engines

Serena Bertagna <sup>1,\*</sup> , Luca Braidotti <sup>1</sup> , Erik Laurini <sup>1</sup>, Alberto Marinò <sup>1</sup> , Sabrina Pricl <sup>1,2</sup>   
and Vittorio Bucci <sup>1</sup> 

<sup>1</sup> Department of Engineering and Architecture, University of Trieste, Via A. Valerio 10, 34127 Trieste, Italy

<sup>2</sup> Department of General Biophysics, Faculty of Biology and Environmental Protection, University of Lodz, ul. Pomorska 141/143, 90-236 Lodz, Poland

\* Correspondence: sbertagna@units.it

**Abstract:** Metal replacements for automotive and aerospace components are already a consolidated reality, in light of the advantages offered by fibre-reinforced polymers, consisting of reduced costs, weight, and environmental impact. As a result, engineering has been studying the possibility of replacing currently used metallic alloys with alternative materials, such as thermoplastic fibre-reinforced polymers, in the manufacturing of non-structural sections of marine engines. Given the peculiar characteristics of the working environment of such parts, i.e., ship engine spaces, and the strict requirements regarding safety, the selection of the polymer must be properly performed through a tailored material design process. Consequently, the redesign of the components must be carried out with the aim of exploiting the best of the materials' properties while ensuring the correct resistance and simplifying installation operations. In this framework, finite element simulations may represent a suitable approach to validate the conformity of the proposed material and design. In this paper, this methodology is applied to a camshaft cover of a four-stroke marine engine, currently made of aluminium alloy. A 30% wt GFs/PA6,6 was identified as the most promising material and the novel plastic cover proved to guarantee the correct resistance while ensuring an important reduction in weight, processing costs, and required energy.

**Keywords:** metal replacement; material design; marine engines; non-structural components; FE analysis



**Citation:** Bertagna, S.; Braidotti, L.; Laurini, E.; Marinò, A.; Pricl, S.; Bucci, V. Thermoplastic Materials for the Metal Replacement of Non-Structural Components in Marine Engines. *Appl. Sci.* **2022**, *12*, 8766. <https://doi.org/10.3390/app12178766>

Academic Editor: Abílio Manuel Pinho de Jesus

Received: 9 August 2022

Accepted: 29 August 2022

Published: 31 August 2022

**Publisher's Note:** MDPI stays neutral with regard to jurisdictional claims in published maps and institutional affiliations.



**Copyright:** © 2022 by the authors. Licensee MDPI, Basel, Switzerland. This article is an open access article distributed under the terms and conditions of the Creative Commons Attribution (CC BY) license (<https://creativecommons.org/licenses/by/4.0/>).

## 1. Introduction

The use of metallic materials for the construction of structural elements has always accompanied technological evolution. The strength, stiffness, and hardness of these materials allow for the manufacture of objects able to withstand heavy loads and stresses, such as those required inside vehicles and machinery [1].

However, within industrial sectors, optimising energy use and reducing weight have become focal points for component manufacturers [2–4]. In this framework, synthetic materials based on either thermoplastic or thermosetting fibre-reinforced polymers (FRPs) have aroused great interest and have been used successfully for metal-replacement applications [5–7]. Indeed, through the years, the technology of such materials has made great strides and is now able to combine elevated mechanical performances with lightness, resistance, durability, and cost-saving in comparison with metallic alloys commonly used for specific components [8]. In addition, it is worth considering the ease of malleability of these polymers, which give designers quite a high freedom in choosing particular and advantageous shapes. All these aspects have contributed to an increased demand for FRPs even outside automotive and aerospace engineering where they found their first applications [9–14].

This diffusion can also be attributed to the implementation of extremely efficient material-processing techniques capable of fully exploiting their potential. Indeed, from the

combined development of raw materials and injection-moulding technologies, a significant return on investment regarding both production time and costs has been achieved. The economic return is even more evident for industrial applications that imply medium–high productivity, in which moulding and thermoforming processes are undisputed leaders [15,16]. Since such two methods apply to thermoplastic polymers, these clearly represent products affected by the major developments.

As a consequence of the increased performance characteristics in thermoplastic FRPs, the marine engineering sector also started investigating their possible applications in place of aluminium alloy for the production of machinery non-structural components. Specifically, attention has been focused on engine parts such as protective covers for valves and mechanisms so far [17]. For such applications, a proper analysis of the working environment is of utmost importance. Ship engine spaces are characterised by high temperatures, moisture content, and chemical agents, which can affect and reduce the mechanical properties of the materials employed and components may be subjected to high loads of both pressure and force. Furthermore, such spaces must guarantee elevated safety standards, and every single element must be assessed and verified in compliance with specific and strict rules and requirements [17]. Consequently, an adequate material design able to ensure resistance to both environmental and loading conditions is a crucial step.

Under this perspective, computer-assisted multiscale material design (CAMMD) has an apparent appeal as a technology with a significant potential influence on both material and process design and innovation. Incorporating CAMMD into the design and/or optimization of new materials and processes can offer a number of benefits including, among others: Speeding up product development by eliminating expensive iterations of trial-and-error rounds, cutting expenditures by implementing innovations throughout the entire pipeline, and decreasing the number of high-cost, large-scale experiments. In addition, *in silico* approaches provide a good chance to anticipate complicated material behaviour and performance across a nearly limitless variety of situations, even some that are impractical to test in real life.

In order to extend the study regarding metal replacement to other marine engine non-structural components, the present paper applies CAMMD principles to compare different fibre-reinforced polymers and identify the most proper alternative to aluminium alloy. For the purposes of the research, a camshaft cover of a marine four-stroke engine was selected as a case study. A metal replacement applied to such components may provide great advantages in terms of the inspection and maintenance operations of an engine's internal spaces; indeed, the novel plastic covers would present a reduced weight and would facilitate handlings and substitutions. Furthermore, the camshaft cover is one of the most numerous components on four-stroke engines, as their quantity depends on the number of cylinders of the considered machinery. Therefore, the replacement of aluminium alloy with a proper FRP would result in significant cost-saving due to the less expensive production process involved. The use of fibre-reinforced thermoplastic materials in the manufacture of camshaft covers could also offer benefits in terms of environmental impact and life cycle assessment [18]. Besides, aluminium die-casting, due to the very rapid solidification of metal, requires very high processing temperatures, extreme injection speeds, and, accordingly, short injection times [19]. The lower processing temperatures required in the machinery could represent an argument to prefer plastic injection moulding [20].

The component selected for the study was completely redesigned by taking into account the properties of the novel material, consisting of 30% wt GFs/PA6,6, in order to ensure the same resistance as its conventional metallic component. Its geometry was adapted by pursuing the aim of limiting the modifications necessary for installation on the engine block. Then, its behaviour was assessed through static linear finite element (FE) simulations able to reproduce the real working environment and conditions. In such a way, an in-depth finite element analysis (FEA), performed with the commercial software ANSYS® Workbench 2020 R2 (ANSYS® Inc., Canonsburg, PA, USA), allowed a

preliminary assessment of both the material's and the redesigned component's performance and validated their use for the searched aims.

## 2. Materials and Methods

### 2.1. Materials

#### 2.1.1. Material Design

The adopted CAMDD-based workflow is based on the adaptation and implementation of a series of computational recipes we previously developed and validated for a range of different (nano)composite polymeric materials [21,22]. Briefly, using the Rotational Isomeric State (RIS) approach [23] at room temperature, 3 independent chain configurations were constructed beginning from the optimum monomer unit for each polymer. Then, for each chain, a three-dimensional (3D) simulation cell was constructed and optimized under periodic boundary conditions (PBCs), either using just polymer chains or 1 filler surrounded by the required amount of polymer molecules to attain a specific weight fraction (see below). As a result, 3 distinct 3D systems were created for each macromolecule generated via RIS, and each of these boxes was subjected to the computational procedure for determining the specified attribute. Accordingly, the reported value of each material property is averaged across three such simulations. All molecular in silico experiments were performed on our own CPU/GPU cluster exploiting the highly parallel features of the open-source platform LAMMPS (<http://lammmps.sandia.gov/>). The COMPASS force field was adopted in all simulations [24]. All theory and simulation details/procedures are given in full in Appendix A.

For the current application, the following systems were considered: System 1) Nylon 6 (PA6) loaded either with glass fibres (GFs) or carbon fibres (CFs); system 2) Nylon 6,6 (PA6,6) loaded either with glass fibres (GFs) or carbon fibres (CFs); system 3) poly(ether ether ketone) (PEEK) loaded with multi-wall carbon nanotubes (MWCNTs), and system 4) PEEK loaded with hydroxyapatite (HA). Systems 1 and 2 were selected as the best compromise between the potential cost and performance; PEEK was selected as the best compromise between performance and eco-compatibility; finally, system 4 was selected on the basis of the best eco-compatibility characteristics of both the polymeric matrix and filler. Furthermore, the choice of thermoplastic polymers mentioned above was based on several considerations, including good thermal and mechanical properties, market and price motivations, easy processability, and material recycling potential. The selected fillers are all endowed with excellent mechanical characteristics and can, at least in principle, impart elevated performance to the corresponding (nano)composite even when added in small amounts. In polymer (nano)composite systems, nanofillers are not regularly aligned in a determined direction but are randomly three-dimensionally distributed in the polymer matrix, then ensuring a macroscopically isotropic behaviour in the system. As a result, the isotropic behaviour assumption for the investigated materials is acceptable.

The results obtained from the application of the CAMMD-based workflow for the prediction of mechanical properties—expressed via the value of the Young modulus  $E$ —for the different polymer (nano)composite systems considered are gathered in Figure 1 and Tables A1–A3.

Figure 1A,B show that in the case of PA6 as the thermoplastic polymeric matrix (system 1) the predicted value of the Young modulus  $E$  significantly increases with filler content, reaching the values of  $4.6 \pm 0.3$  GPa ( $E_f = 4.2$ ) and  $9.1 \pm 0.2$  GPa ( $E_f = 8.3$ ) in the presence of 30% wt of GFs and CFs, respectively (Table A1). Simulations of the PA6,6-based systems (system 2) yielded analogous results, although, with respect to the corresponding PA6-based (nano)composites, higher values of  $E$  (and  $E_f$ ) are predicted at all filler concentrations considered, as shown in Figure 1C,D. Taking again a fibre content of 30% wt for comparison, the predicted value of the Young modulus (and  $E_f$ ) for the relevant PA6,6/GFs and PA6,6/CFs systems are  $10.2 \pm 0.5$  GPa ( $E_f = 4.1$ ) and  $22.1 \pm 0.9$  GPa ( $E_f = 8.8$ ), respectively (Table A2). Simulations of systems 3 and 4, consisting of a PEEK matrix loaded with different amounts of MWCNTs or HA, respectively, revealed that—by

virtue of the high value of the Young modulus of the pristine polymer ( $4.2 \pm 0.2$  GPa, Table A3) —a similar and remarkable increase in this property could be observed at lower filler amounts in both cases (Figure 1E,F). As an example, the values of  $9.6 \pm 0.2$  GPa ( $E_f = 2.3$ ) and  $9.8 \pm 0.4$  GPa ( $E_f = 2.3$ ) are predicted for PEEK loaded with 20% wt of MWCNTs and HA, respectively (Table A3). Combined with the additional economic and ecologic/sustainability considerations (e.g., achieving the best agreement between costs, material performance, and the viability of mechanical, thermal, and solvolytic recycling), these findings led to the selection of the system based on PA6,6 loaded with 30% wt glass fibres as the material component for the re-design camshaft cover application.

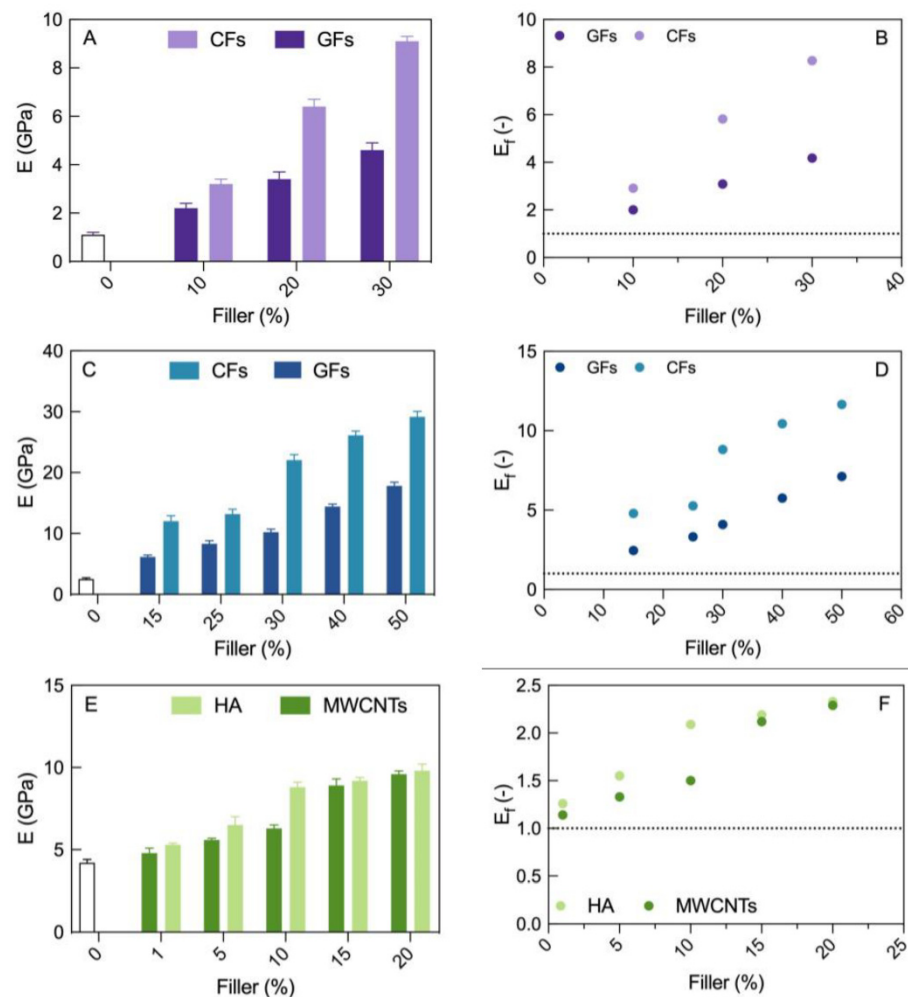


**Figure 1.** CAMMD-based predicted values of the Young modulus  $E$  (A,C,E) and the corresponding enhancement factor  $E_f (=E$  of the (nano)composite/ $E$  of the pristine polymeric matrix) (B,D,F) for the different polymer/filler systems as a function of fibre loading (% wt). (A,B): PA6 loaded with GFs or CFs; (C,D): PA6,6 loaded with GFs or CFs; (E,F): PEEK loaded with MWCNTs or HA.

### 2.1.2. Case-Study Component: Camshaft Cover

A camshaft cover is a non-structural component aimed at allowing inspection and maintenance operations of the camshaft chamber while preserving it from external dust. The exterior surface of the component is exposed to the engine-space environment, characterized by a moisture content of about 50–80% and a room temperature higher than  $40$  °C, while the interior surface is exposed to an atmosphere saturated with oil particles and temperatures less than  $80$  °C. The camshaft cover is currently made of aluminium alloy and fabricated through the die-casting process. The cover is fixed to the engine casing by means of four tightening bolts, and the sealing is ensured by a gasket.

The component is subject to the pressure coming from the camshaft chamber which may vary from 0.05 to 1 bar, as evaluated from the real working conditions. This variation in pressure is due to the rotation of the crankshaft located in a space communicating with the camshaft chamber. The expected lifetime of the reference camshaft cover is approximately equal to 10 years; consequently, it should be replaced three times during the engine's lifetime.

## 2.2. Methods

### 2.2.1. Model Redesign and Material Characterisation

The nano-engineered plastic 30% wt GFs/PA6,6 was selected on the basis of the outcomes of the material design phase.

The redesign of the component (Figure 2) was carried out with the aim to ensure the model has a proper structural strength according to the mechanical properties of the selected FRP. In order to avoid high thicknesses and consequent warping phenomena during injection moulding, the entire internal face of the camshaft cover is shaped with a grillage of ribs, whereas on the external face there are shorter ribs only along the edge.

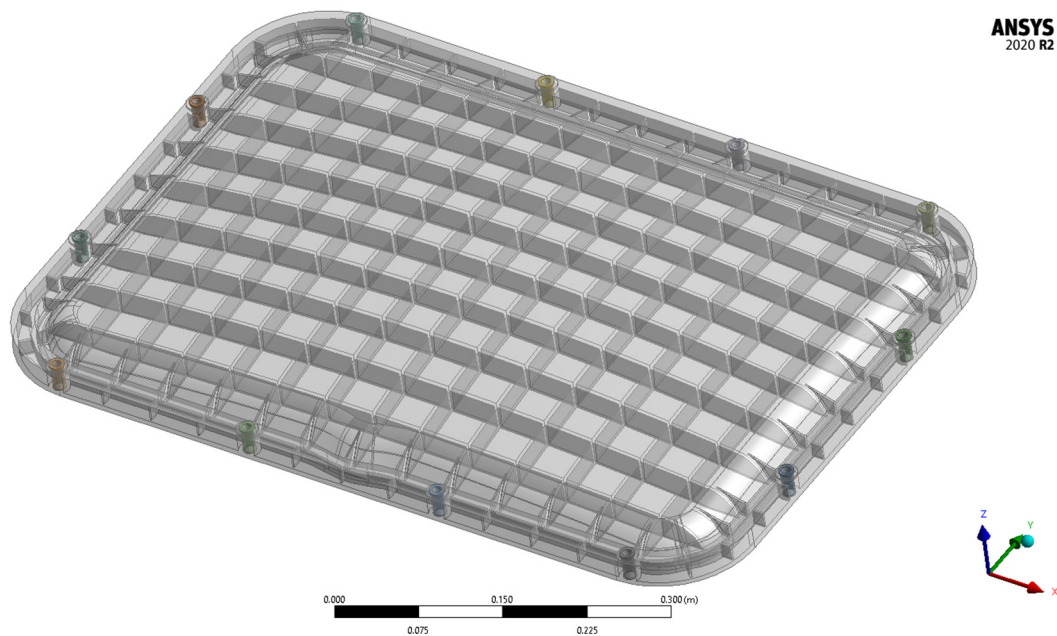


**Figure 2.** Redesigned camshaft cover in 30% wt GFs/PA6,6.

Due to the reduced mechanical characteristics of the plastic material selected and to guarantee the sealing exerted by the gasket, the number of tightening spots between the component and the engine casing was increased. The redesigned component presents 12 studs located in as many S355-steel sleeves. These allow for fixing the cover to the engine block by preserving the studs to apply their full tightening pressure on the edge of the cover itself. Furthermore, the sleeves' neck prevents the component from moving and ensures the maintenance of the correct position.

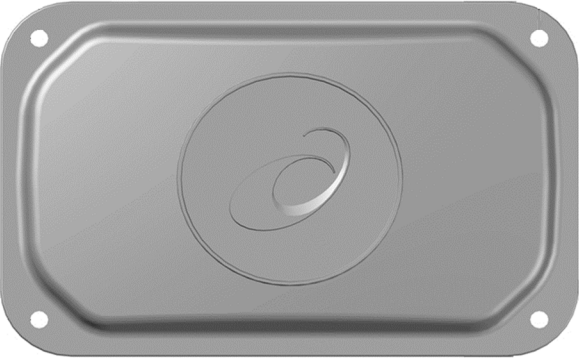
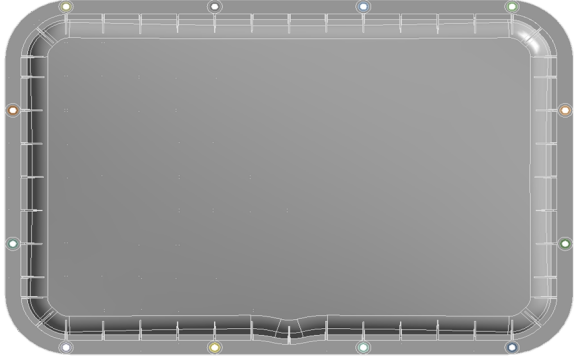
Table 1 shows the properties of both 30% wt GFs/PA6,6 (from Table A2 and [17]) and S355 steel [25]. Table 2 shows a comparison between the reference and the redesigned component, highlighting the most significant differences.



**Table 1.** Isotropic linear elastic properties of 30% wt GFs/PA6,6 and S355 steel at room temperature.

Property	30% wt GFs/PA6,6	S355 Steel [25]
Young Modulus (E, GPa)	10.2 ± 0.5	205
Poisson's ratio ( $\nu$ )	0.4	0.29
Density ( $d$ , kg/m <sup>3</sup> )	1320 ± 30	7850
Strain at break (%)	4 ± 0.2	15.55
Stress at break (MPa)	189 ± 6	514

**Table 2.** Comparison between reference and redesigned component.

Reference Camshaft Cover	Redesigned Camshaft Cover
	
Material: Aluminium alloy Working process: Die-casting 4 tightening bolts Mass: 13.3 kg	Material: 30% wt GFs/PA6,6 Working process: Injection moulding 12 tightening studs Mass: 4.8 kg

### 2.2.2. Finite Element Simulations

Static linear FE simulations were performed by using the Mechanical suite of the commercial FEA software ANSYS<sup>®</sup> Workbench 2020 R2. Both the plastic cover and the steel sleeves were modelled as 3D solid bodies, while the studs were not considered in the analysis. These in fact exert their pressure directly on the sleeve, and only a negligible part of this pressure is transmitted to the cover through the neck of the sleeve. Moreover, the engine block was not modelled, as it was unnecessary due to the high difference in stiffness of the materials involved (i.e., FRP and steel). As regards the gasket, this was not modelled but its compression was calculated through laboratory tests and inserted as a pressure load for the purpose of the simulations [26].

For both the cover and the sleeves, the materials were properly characterised as being isotropic and linear through the data reported in Table 1.

In order to reduce computational times and efforts, symmetry regions were applied; in fact, the geometry of the model is not perfectly symmetrical, but the existence of two ideal planes of symmetry could be hypothesised in correspondence with the XZ and YZ planes. In order to take into account the worst condition possible, the authors focused the analysis on the part of the cover where the tightening studs are most spaced apart. Therefore, for the purposes of calculation, the model was reduced to a quarter of the entire camshaft cover, as shown in Figure 3.

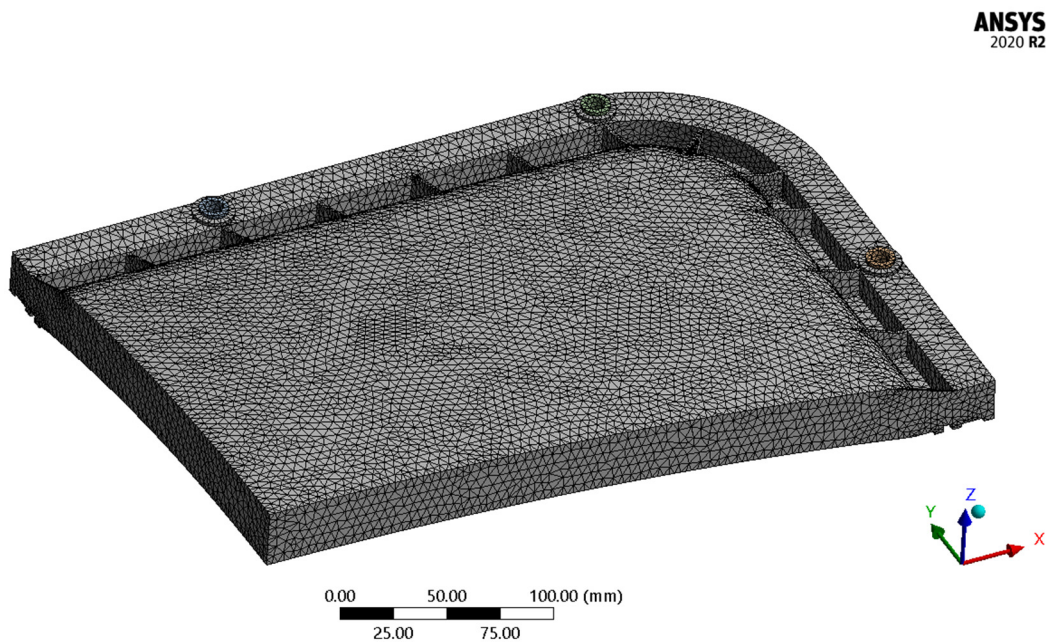


**Figure 3.** Mesh.

The mesh consisted of an unstructured grid employing 3D tetrahedral elements; these are 3D 20-node second-order structural solid elements, also called bricks. Each node has three translational degrees of freedom. Such elements support plasticity, hyperelasticity, creep, stress-stiffening, large deflection, and large strain capabilities. The mesh was optimized in the proximity of geometry changes and curvatures (Figure 3). The largest size of a single mesh element corresponded to the component's maximum local thickness, which is 3 mm. Table 3 shows the main properties of the mesh in terms of characteristics and control metrics used to validate the grid.

**Table 3.** Mesh properties for the FE camshaft-cover model.

Property	Value	Explanation
Element size	3 mm	-
Number of elements	109,778	-
Number of nodes	201,558	-
Element quality (average value)	0.708	Metric based on the ratio of the volume to the edge length for a given element (optimal values within 0.5 ÷ 1.0)
Aspect ratio (average value)	2.361	Ratio of longest to the shortest side in an element (optimal values within 1 ÷ 5)

The model was considered fully fixed by constraining all the degrees of freedom at the base of the steel sleeves, in order to reproduce the real situation in which the cover is tightened on the engine block. Besides, two different contact conditions were imposed between the steel sleeves and the plastic cover. A bonded contact was applied between the cover and the neck of the sleeves (Figure 4a), and frictionless contact was applied between the cover and the outer cylindrical surface of the sleeves (Figure 4b). In such a way, the cover can be subjected to small deflections and movements without suffering detachment from the defined base. Indeed, the bonded contact does not allow either sliding or separation between the faces to which it is applied, whereas the frictionless contact does not prevent the separation between faces but allows them to slide in a tangential direction, without considering any frictional force.

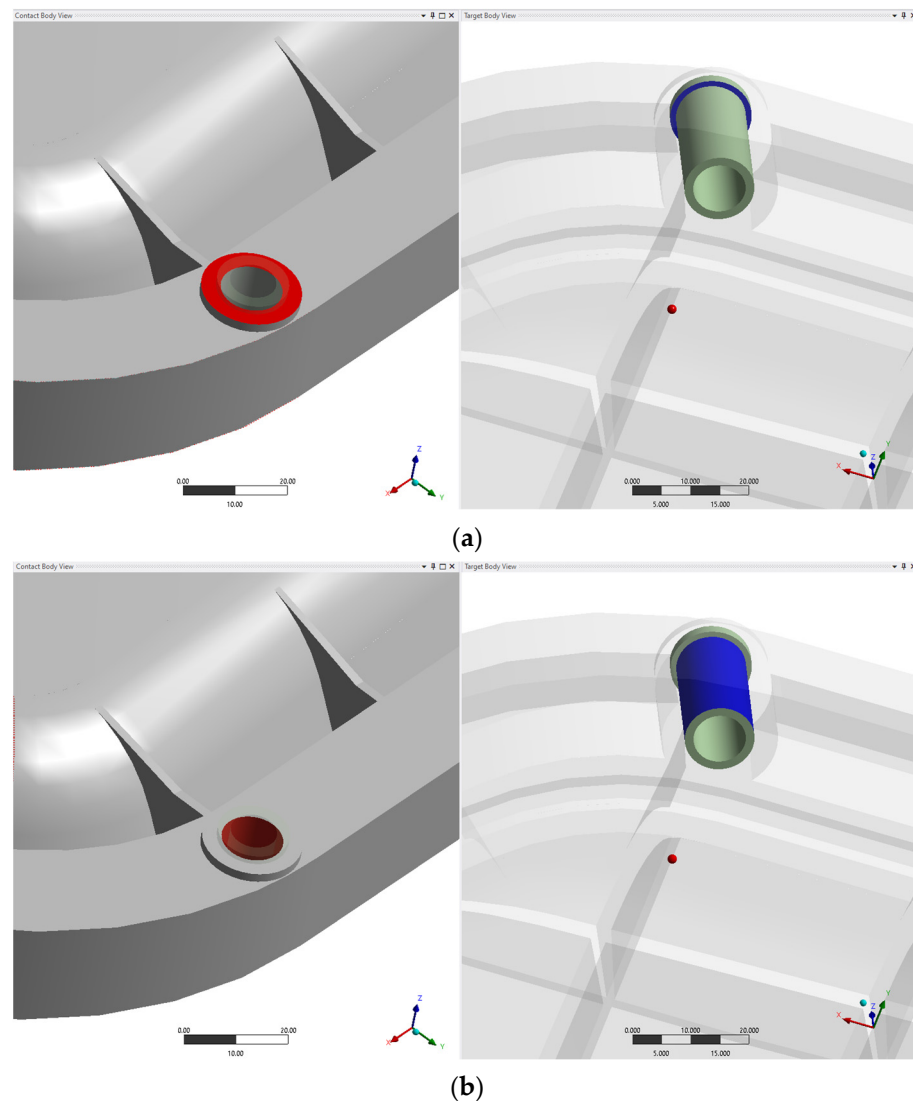


**Figure 4.** (a) Bonded contact condition; (b) Frictionless contact condition.

As regards the load condition, the model was assessed by applying both a pressure load equal to 0.01 MPa on the internal face of the camshaft cover (corresponding to the internal crankcase pressure) and a pressure load equal to 0.2634 MPa on the gasket housing (corresponding to the pressure exerted by the gasket on the cover) (Figure 5). Both values were derived from laboratory tests and measurements carried out in a real working environment.



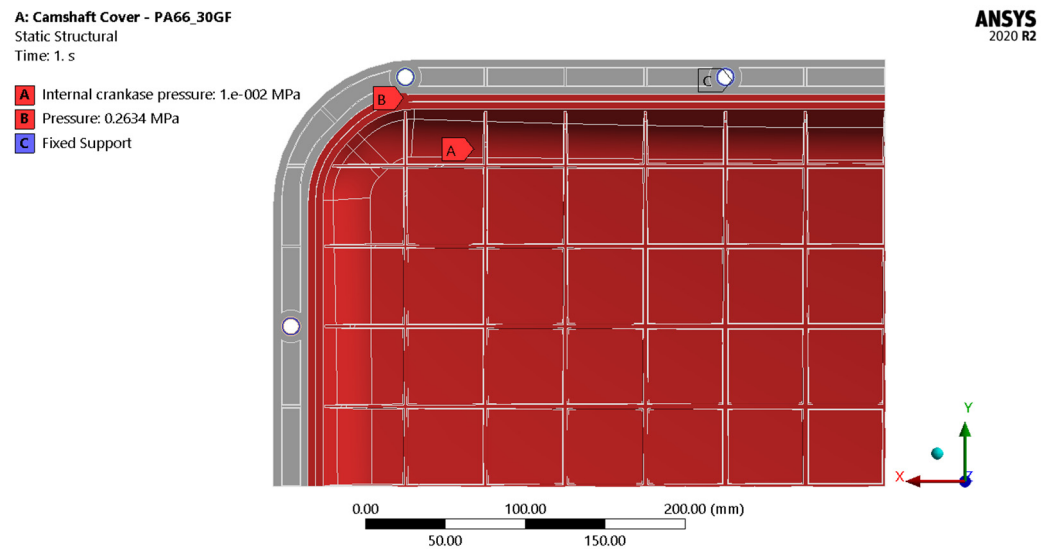


**Figure 5.** Loads and constraints condition.

### 3. Results and Discussion

The results obtained from the static linear finite element simulations are extensively discussed in the following and summarised in Table 4, with a comparison to threshold values when available.

**Table 4.** FEA results for the camshaft cover vs. threshold values.

	FEA Result	Threshold Value
Total deformation (mm)	0.299	-
Equivalent (von-Mises) stress (MPa)	22.12	189 ± 6
Equivalent elastic strain (%)	0.219	4 ± 0.2
Vertical displacement of the gasket housing (mm)	0.0596	-
Gasket compression value (%)	28.8	15–30

The maximum deformation (Figure 6) caused by the internal crankcase pressure is quite limited and occurs in correspondence with the central area of the cover, which can be considered a safe area since it is far from the tightening spots; then, this gradually decreases towards the external frame of the component, according to the presence of the fixed-support constraint placed on the base surface of the steel sleeves.

A: Camshaft Cover - PA66\_30GF  
 Total Deformation  
 Type: Total Deformation  
 Unit: mm  
 Time: 1

ANSYS  
 2020 R2

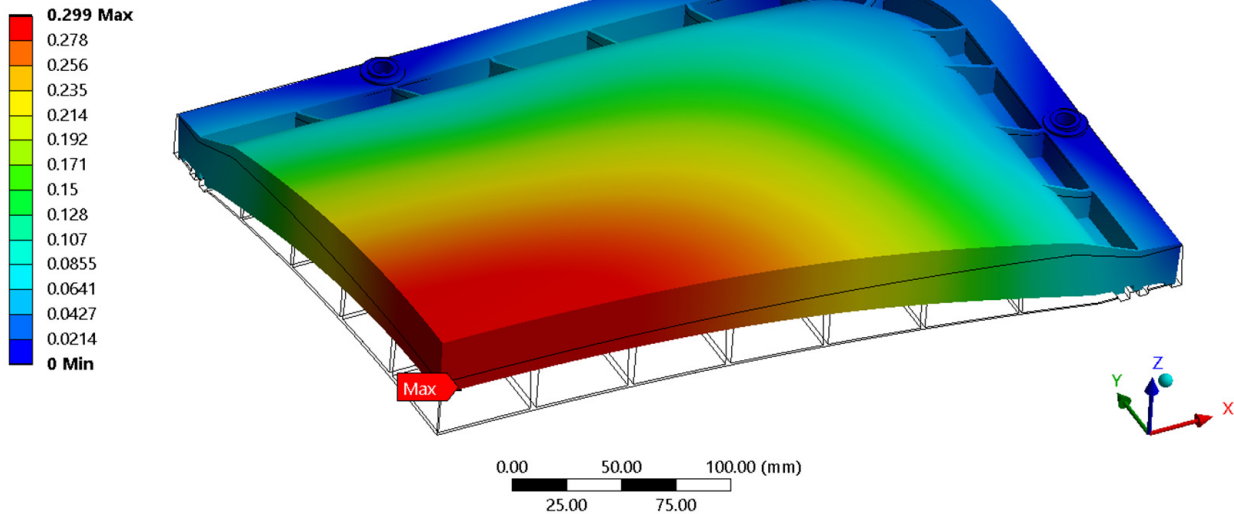
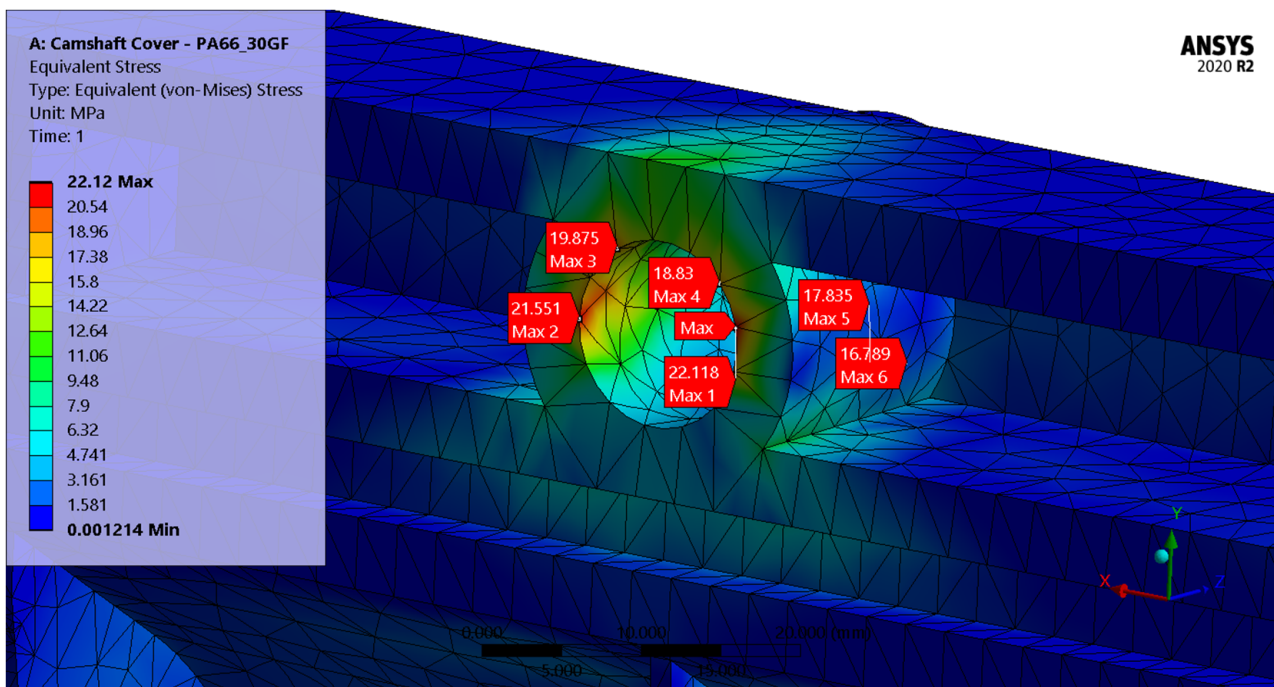


Figure 6. FEA results: total deformation.

As regards the maximum stress and strain (Figure 7), their values are substantially lower than the tolerable limits for the material selected. They occur in correspondence with the tightening spots since the material is more solicited in those points due to the presence of the studs. In particular, the highest values for stress and strain occur in correspondence with the most spaced stud from the adjacent one, as it is subjected to a greater load to ensure the seal of the gasket.



(a)

Figure 7. Cont.

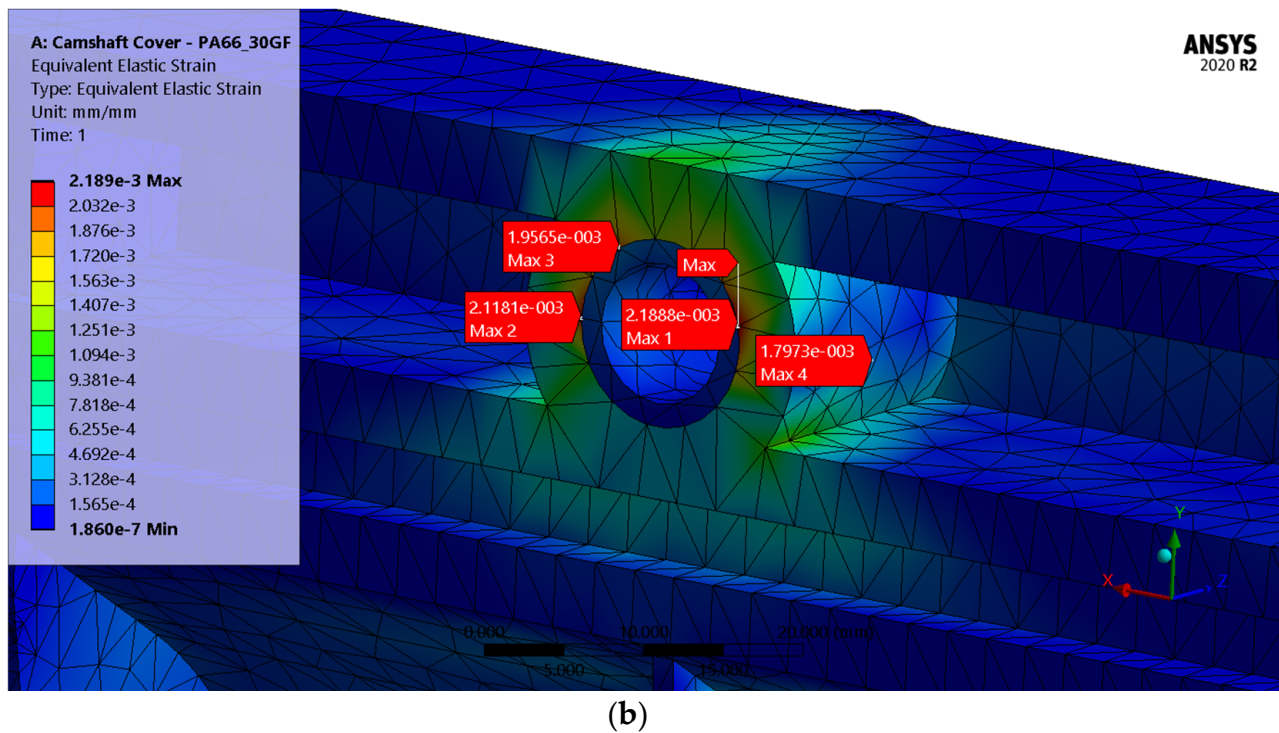


**Figure 7.** FEA results: (a) Equivalent (von-Mises) stress; (b) Equivalent elastic strain.

A further quantity that was calculated during the FE analysis consists of the maximum vertical displacement in correspondence with the gasket housing (Figure 8). Through this result, the compression value  $C$  actually exerted by the gasket when the cover is deformed under the action of the acting pressures was calculated by means of the following equation:

$$C [\%] = \frac{d_{\text{gasket}} - (h_{\text{housing}} + vd)}{d_{\text{gasket}}} 100 \quad (1)$$

in which  $d_{\text{gasket}}$  represents the gasket diameter and is equal to 5 mm;  $h_{\text{housing}}$  represents the height of the gasket housing and is equal to 3.5 mm;  $vd$  represents the vertical displacement in correspondence with the gasket housing evaluated from the FE analysis. The recommended compression value on the gasket for static applications is between 15 and 30%, with 30% the initial value when the vertical displacement of the gasket housing is null and 15% the minimum value able to guarantee the correct sealing of the gasket. On the basis of the results obtained, the compression value  $C$  for the plastic cover is equal to 28.8% and therefore is within the optimal range of operation.

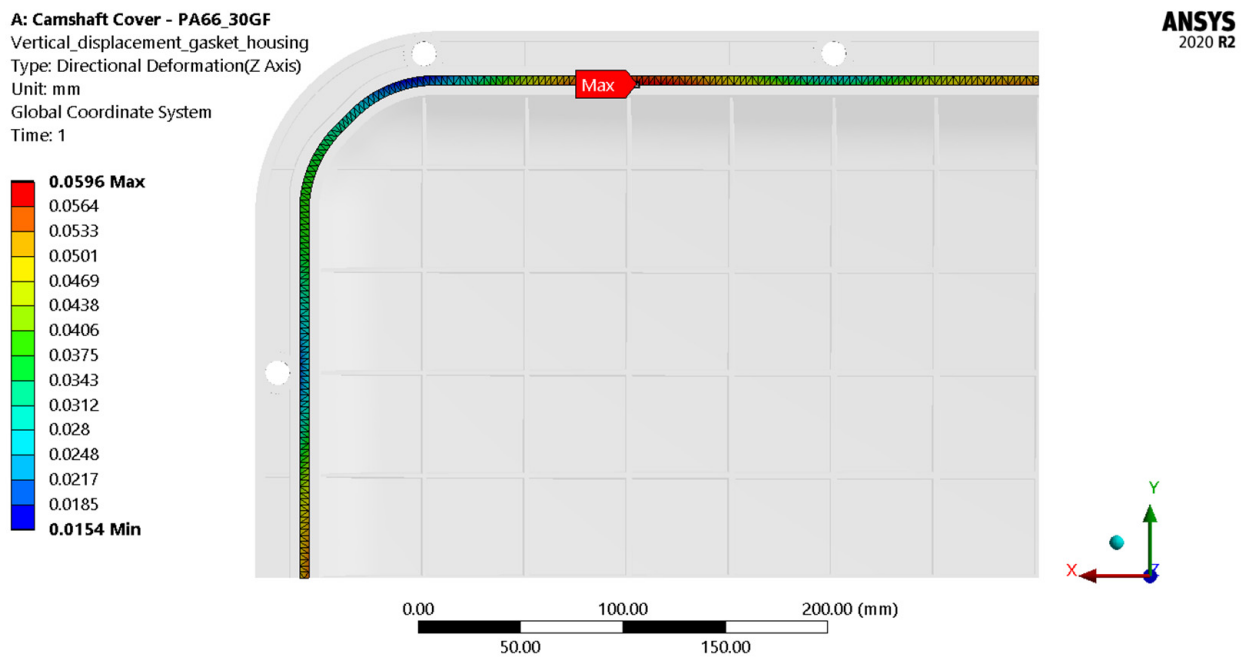


Figure 8. FEA results: vertical displacement on the gasket housing.

#### 4. Conclusions

As one of the most challenging activities in marine engineering, studying the possibility to replace metal components in the production of non-structural sections of marine engines must take into account several aspects associated with the working environment and the safety requirements of international institutions. However, through a proper and extensive material design process, valuable alternatives may be identified in place of conventionally used metallic alloys.

Specifically, in this paper, the authors compared several fibre-reinforced polymers on the basis of their performance, cost, and ease of processing. As a result, PA6,6 loaded with 30% wt of glass fibres turned out to be the most suitable material since it combines both advantageous costs and characteristics, such as being lightweight and high strength. By using this material for the production of the analysed camshaft covers, a potential cost reduction equal to 50% of the cost of the aluminium-alloy cover was estimated. As regards weights, the novel plastic component ensures a reduction greater than 60% of the original weight of the aluminium-alloy cover. This is an element of paramount importance for technical personnel in charge of services and inspections since it allows for the performance of such activities in safer and more comfortable conditions. As an additional consideration, the potential lower environmental footprint of plastic camshaft covers should not be neglected. Even though aluminium is completely recyclable, its reuse at the end of the cover's lifetime could not be granted and plastic covers would be more favourable in terms of life cycle assessment.

In conclusion, the static linear FE simulations underlined the suitability of the selected materials for the research aims, by ensuring good results for all the investigated quantities. However, studies regarding both non-linear behaviour and creep deformation over time are already in progress; indeed, these two aspects are fundamental to verifying the long-term performance of the material and the resistance capacity of the geometry proposed in a hard environment such as ship engine spaces. Such analyses will also allow the estimation of the lifetime of the plastic camshaft covers, which is expected to be comparable to those made of aluminium alloy.

**Author Contributions:** Conceptualization, S.B. and S.P.; methodology, S.B. and S.P.; validation, S.B., E.L. and S.P.; formal analysis, S.B., L.B. and S.P.; investigation, S.B., E.L., S.P. and V.B.; resources, A.M., S.P. and V.B.; data curation, S.B., L.B., E.L. and S.P.; writing—original draft preparation, S.B., L.B., E.L. and S.P.; writing—review and editing, S.B., L.B., E.L., A.M., S.P. and V.B.; visualization, S.B. and S.P.; supervision, A.M., S.P. and V.B.; project administration, A.M., S.P. and V.B.; funding acquisition, A.M., S.P. and V.B. All authors have read and agreed to the published version of the manuscript.

**Funding:** This research was funded by [Regione Autonoma Friuli Venezia Giulia] grant number [J96G17000110005].

**Acknowledgments:** The present work was supported by “PLASTICO–Plastic Cover for Marine Engine” research project, funded by the Regione Autonoma Friuli Venezia Giulia with the program POR-FESR 2014–2020 Asse 1 Azione 1.3b.

**Conflicts of Interest:** The authors declare no conflict of interest.

## Appendix A

### Computational Details

The Berendsen thermostat/barostat [27] with coupling time constants  $\tau_T = 0.1$  s and  $\tau_P = 0.5$  ps was used to handle temperature and pressure control during all MD calculations. To account for short-range intermolecular interactions in the fully atomistic macromolecular models, the Lennard-Jones 9-6 potential function with geometric mean combination criterion was applied. Long-range electrostatic interactions were managed *via* the particle mesh Ewald (PME) [28] method to an accuracy of 0.001 kcal/mol. The length of the simulation cell was used as the cut-off distance for truncating any non-bonded interactions. Unless otherwise specified, all MD runs used the velocity Verlet approach with a 1 fs time step to integrate Newton’s equations of motion. In order to determine the stress-strain relationship for the various polymer/(nano)composite systems, the first step in the simulation protocol consisted in reaching the minimum initial stress state for each equilibrated periodic box obtained as described above. Accordingly, MD simulations in the constant volume-constant temperature (NVT) and constant volume-constant energy (NVE) ensembles were run on each simulation box for 5 ns and 2 ns, respectively. To relieve initial stresses, each unit cell size was then relaxed using constant temperature-constant pressure (NPT) MD simulations (up to several thousand steps in length depending on the size of the simulation box), followed by 2 ns of further MD equilibration of the NVE ensemble. In order to preserve the filler shape, a 0.5% uniform strain field was applied to each equilibrated system along the necessary directions by maintaining the filler coordinates unchanged while proportionally scaling both the unit cell and positions of the atoms along the polymer chains. Each simulation cell was stressed using this computational method to determine the unidirectional tension/compression (UT/C) and hydrostatic tension/compression (HT/C), respectively. During UT/C simulations, one direction was subjected to strain in the first instance, and the procedure was then repeated for the other two directions starting with the unstrained cell. On the other hand, in HT/C simulations, the same strain field was concurrently applied to all normal directions. Stress is expressed at the atomic level as a virial form:

$$\sigma_{ij} = -\frac{1}{V} \sum_a \left( M^a v_i^a v_j^a + \frac{1}{2} \sum_{b \neq a} F_i^{ab} r_j^{ab} \right) \quad (A1)$$

where  $V$  is the simulation cell volume, denoted by the sum of each atom’s volume  $V^a$ ; the  $i$ -th and  $j$ -th components of atom  $a$ ’s velocity are denoted as  $v_i^a$  and  $v_j^a$ , respectively;  $F_i^{ab}$  is the  $i$ -th component of the force between atoms  $a$  and  $b$ ;  $r_j^{ab}$  is the separation between the same two atoms. Tensile stress is to be expressed as a positive amount by the use of the negative sign. Since, in the context of continuum mechanics the assumptions that: (1) the polymer matrix and the pertinent (nano)composites are characterized by material



symmetry, and (2) the linear relationship between stress and strain both hold, the equivalent continuum's generalized constitutive relation is as follows:

$$\begin{Bmatrix} \sigma_{11} \\ \sigma_{22} \\ \sigma_{33} \end{Bmatrix} = \begin{bmatrix} C_{11} & C_{12} & C_{12} \\ C_{12} & C_{11} & C_{12} \\ C_{12} & C_{12} & C_{11} \end{bmatrix} \begin{Bmatrix} \varepsilon_{11} \\ \varepsilon_{22} \\ \varepsilon_{33} \end{Bmatrix} \quad (\text{A2})$$

where  $C_{ij}$  are the elastic constants (stiffness);  $\sigma_{ij}$  and  $\varepsilon_{ij}$  are the stress and strain components, respectively. As mentioned in the main text, a 0.5% strain was applied to the undeformed cell along one direction at a time in order to anticipate stress-strain behaviour under unidirectional tension or compression. The only non-zero strain component in this scenario, using direction 1 as the default, is  $\varepsilon_{11}$ . Expansion of the first row of Equation (A2) yields:

$$\sigma_{11} = C_{11}\varepsilon_{11} \quad (\text{A3})$$

By deforming the cell along directions 2 or 3, identical expressions may be generated. Thus, three distinct values of the elastic constant  $C_{11}$  are obtained for each tension or compression simulation.  $C_{11}$  may be further averaged as the strain is delivered evenly in each direction ( $\varepsilon_{11} = \varepsilon_{22} = \varepsilon_{33}$ ). The elastic bulk modulus  $K$  under hydrostatic tension and compression is given by Equation (A4):

$$K = \frac{1}{3} \left( \frac{\sigma_{11} + \sigma_{22} + \sigma_{33}}{\varepsilon_{11} + \varepsilon_{22} + \varepsilon_{33}} \right) \quad (\text{A4})$$

Consequently, by noting that  $\varepsilon_{ii}$  is equal to 0.05 along all directions,  $K$  can be simply calculated using Equation (A4) by inputting the normal stress components generated from the appropriate simulations.

Lastly, the essential correlations between the elastic constant  $C_{11}$ , the bulk modulus  $K$ , the elastic (Young) modulus  $E$ , and the Poisson's ratio  $\nu$  that is:

$$C_{11} = \frac{(1 - \nu)E}{(1 + \nu)(1 - 2\nu)} \quad (\text{A5})$$

$$K = \frac{E}{3(1 - 2\nu)} \quad (\text{A6})$$

allow the estimation of the values for  $\nu$  and  $E$  after  $K$  and  $C_{11}$  are obtained as a consequence of the simulation processes described before.

**Table A1.** Values of the Young modulus  $E$  and the corresponding enhancement factor  $E_f$  ( $=E$  of the (nano)composite/ $E$  of the pristine polymeric matrix) for the system based on Nylon 6 (PA6) and different loadings of glass fibres (GFs) or carbon fibres (CFs) (system 1).

System	E (GPa)	$E_f$ (-)	System	E (GPa)	$E_f$ (-)
PA6	1.1 ± 0.1				
10% wt GFs/PA6	2.2 ± 0.2	2.0	10% wt CF/PA6	3.2 ± 0.2	2.9
20% wt GFs/PA6	3.4 ± 0.3	3.1	20% wt CF/PA6	6.4 ± 0.3	5.8
30% wt GFs/PA6	4.6 ± 0.3	4.2	30% wt CF/PA6	9.1 ± 0.2	8.3

**Table A2.** Values of the Young modulus E and the corresponding enhancement factor  $E_f$  (=E of the (nano)composite/E of the pristine polymeric matrix) for the system based on Nylon 6,6 (PA6,6) and different loadings of glass fibres (GFs) or carbon fibres (CFs) (system 2).

System	E (GPa)	$E_f$ (-)	System	E (GPa)	$E_f$ (-)
PA6,6	2.5 ± 0.2				
10% wt GFs/PA6,6	6.1 ± 0.3	2.5	10% wt CF/PA6,6	12.0 ± 0.9	4.8
20% wt GFs/PA6,6	8.3 ± 0.5	3.3	20% wt CF/PA6,6	13.2 ± 0.8	5.3
30% wt GFs/PA6,6	10.2 ± 0.5	4.1	30% wt CF/PA6,6	22.1 ± 0.9	8.8
40% wt GFs/PA6,6	14.4 ± 0.4	5.8	40% wt CF/PA6,6	26.1 ± 0.7	10.4
50% wt GFs/PA6,6	17.8 ± 0.6	7.1	50% wt CF/PA6,6	29.1 ± 0.9	11.7

**Table A3.** Values of the Young modulus E and the corresponding enhancement factor  $E_f$  (=E of the (nano)composite/E of the pristine polymeric matrix) for the system based on poly(ether ether ketone) (PeeK) and different loadings of multi-wall carbon nanotubes (MWCNTs) hydroxyapatite (HA) (systems 3 and 4).

System	E (GPa)	$E_f$ (-)	System	E (GPa)	$E_f$ (-)
PEEK	4.2 ± 0.2				
1% wt MWCNTs/PEEK	4.8 ± 0.3	1.1	1% wt HA/PEEK	5.3 ± 0.1	1.3
5% wt MWCNTs/PEEK	5.6 ± 0.1	1.3	5% wt HA/PEEK	6.5 ± 0.5	1.6
10% wt MWCNTs/PEEK	6.3 ± 0.2	1.5	10% wt HA/PEEK	8.8 ± 0.3	2.1
15% wt MWCNTs/PEEK	8.9 ± 0.4	2.1	15% wt HA/PEEK	9.2 ± 0.2	2.2
20% wt MWCNTs/PEEK	9.6 ± 0.2	2.3	20% wt HA/PEEK	9.8 ± 0.4	2.3

## References

- Mridha, S. Metallic Materials. In *Reference Module in Materials Science and Materials Engineering*; Elsevier: Amsterdam, The Netherlands, 2016; p. B9780128035818041000. ISBN 978-0-12-803581-8.
- Pruez, J.; Shoukry, S.; Williams, G.; Shoukry, M. *Lightweight Composite Materials for Heavy Duty Vehicles*; West Virginia University: Morgantown, WV, USA, 2013.
- Merulla, A.; Gatto, A.; Bassoli, E.; Munteanu, S.I.; Gheorghiu, B.; Pop, M.A.; Bedo, T.; Munteanu, D. Weight Reduction by Topology Optimization of an Engine Subframe Mount, Designed for Additive Manufacturing Production. *Mater. Today Proc.* **2019**, *19*, 1014–1018. [[CrossRef](#)]
- Lutsey, N. *Review of Technical Literature and Trends Related to Automobile Mass-Reduction Technology*; Institute of Transportation Studies: Davis, CA, USA, 2010.
- Burgmann, B. Bell Injection Moulding. Savings all round with metal replacement programme. *Seal. Technol.* **2009**, *7*, 4–5. [[CrossRef](#)]
- Fragassa, C. Lightning Structures by Metal Replacement: From Traditional Gym Equipment to an Advanced Fiber-Reinforced Composite Exoskeleton. *Facta Univ. Ser. Mech. Eng.* **2021**, *19*, 155. [[CrossRef](#)]
- Davies, J.I.; Humphris, K.J. Metal Replacement by Shortfibre-Reinforced Thermoplastics: A Case Study. *Plast. Rubber Mater. Appl.* **1980**, *5*, 25–31.
- Nagavally, R.R. Composite Materials—History, Types, Fabrication Techniques, Advantages, and Applications. *Int. J. Adv. Sci. Eng. Technol.* **2016**, *4*, 87–92.
- Do, M.D.; Kim, M.; Nguyen, D.; Han, S.; Pham Van, H.; Choi, H.-J. Multistep Workpiece Localization with Automated Symmetry Identification for Aerospace Carbon Fiber Reinforced Plastic Components. *Int. J. Precis. Eng. Manuf.-Green Technol.* **2021**, *9*, 1133–1150. [[CrossRef](#)]
- Zhao, J.; Yu, S.; Chen, G.; Juay, Y. *Over Moulding Technologies for Automotive Plastic Components Manufacturing Applications*; SIMTech Technical Reports; Citeseer: State College, PA, USA, 2008; Volume 9.
- Pashte, S.; Wagle, K.; Agrawal, S.; Sudhakar, D.S.S.; Patil, B.; Singraur, D.S. Simulation and Optimization for a Plastic Component. *IOP Conf. Ser. Mater. Sci. Eng.* **2020**, *872*, 012072. [[CrossRef](#)]
- McCann, K. Nanocomposites: The Future of Automotive Plastics. *AutoTechnology* **2001**, *1*, 50–51. [[CrossRef](#)]
- Greene, J. Design Aspect. In *Automotive Plastics and Composites*; Elsevier: Amsterdam, The Netherlands, 2021; pp. 301–324. ISBN 978-0-12-818008-2.
- Ioan, T.; Besliu, I.; Amarandei, D. Application of Reverse Engineering for Automotive Plastic Components—Case Study. *Macromol. Symp.* **2021**, *395*, 2000265. [[CrossRef](#)]
- Barbosa, R.C.N.; Campilho, R.D.S.G.; Silva, F.J.G. Injection Mold Design for a Plastic Component with Blowing Agent. *Procedia Manuf.* **2018**, *17*, 774–782. [[CrossRef](#)]

16. Wang, C.; Huang, M.; Shen, C.; Zhao, Z. Warpage Prediction of the Injection-Molded Strip-like Plastic Parts. *Chin. J. Chem. Eng.* **2016**, *24*, 665–670. [[CrossRef](#)]
17. Bertagna, S.; Laurini, E.; Marinò, A.; Nasso, C.; Pricl, S.; Bucci, V. Design of Non-Structural Components for Marine Engines Based on Nano-Engineered Thermoplastic Polymers. *Int. Shipbuild. Prog.* **2019**, *66*, 163–180. [[CrossRef](#)]
18. Mio, A.; Bertagna, S.; Cozzarini, L.; Laurini, E.; Bucci, V.; Marinò, A.; Fermeglia, M. Multiscale Modelling Techniques in Life Cycle Assessment: Application to Nanostructured Polymer Systems in the Maritime Industry. *Sustain. Mater. Technol.* **2021**, *29*, e00327. [[CrossRef](#)]
19. Watkins, M.F.; Mani, M.; Lyons, K.W.; Gupta, S.K. Sustainability Characterization for Die Casting Process. In Proceedings of the ASME 2013 International Design Engineering Technical Conferences and Computers and Information in Engineering Conference, Portland, AZ, USA, 4–7 August 2013.
20. Dimla, D.E.; Camilotto, M.; Miani, F. Design and Optimisation of Conformal Cooling Channels in Injection Moulding Tools. *J. Mater. Process. Technol.* **2005**, *164–165*, 1294–1300. [[CrossRef](#)]
21. Fermeglia, M.; Mio, A.; Aulic, S.; Marson, D.; Laurini, E.; Pricl, S. Multiscale Molecular Modelling for the Design of Nanostructured Polymer Systems: Industrial Applications. *Mol. Syst. Des. Eng.* **2020**, *5*, 1447–1476. [[CrossRef](#)]
22. Laurini, E.; Marson, D.; Fermeglia, M.; Pricl, S. Multimodel Approach for Accurate Determination of Industry-Driven Properties for Polymer Nanocomposite Materials. *J. Comput. Sci.* **2018**, *26*, 28–38. [[CrossRef](#)]
23. Helfer, C.A.; Mattice, W.L. The Rotational Isomeric State Model. In *Physical Properties of Polymers Handbook*; Mark, J.E., Ed.; Springer: New York, NY, USA, 2007; pp. 43–57. ISBN 978-0-387-31235-4.
24. Sun, H. COMPASS: An Ab Initio Force-Field Optimized for Condensed-Phase Applications Overview with Details on Alkane and Benzene Compounds. *J. Phys. Chem. B* **1998**, *102*, 7338–7364. [[CrossRef](#)]
25. Corigliano, P.; Cucinotta, F.; Guglielmino, E.; Risitano, G.; Santonocito, D. Thermographic Analysis during Tensile Tests and Fatigue Assessment of S355 Steel. *Procedia Struct. Integr.* **2019**, *18*, 280–286. [[CrossRef](#)]
26. Trelleborg Sealing Solutions. *O-Rings and Back-Up Rings*; Trelleborg Sealing Solutions: Trelleborg, Sweden, 2016.
27. Berendsen, H.J.C.; Postma, J.P.M.; van Gunsteren, W.F.; DiNola, A.; Haak, J.R. Molecular Dynamics with Coupling to an External Bath. *J. Chem. Phys.* **1984**, *81*, 3684–3690. [[CrossRef](#)]
28. Toukmaji, A.; Sagui, C.; Board, J.; Darden, T. Efficient Particle-Mesh Ewald Based Approach to Fixed and Induced Dipolar Interactions. *J. Chem. Phys.* **2000**, *113*, 10913–10927. [[CrossRef](#)]